

A Framework for the Experimental Comparison of Solar and Skydome Illumination

Joseph T. Kider Jr.

Daniel Knowlton

Jeremy Newlin

Yining Karl Li

Donald P. Greenberg

Program of Computer Graphics, Cornell University

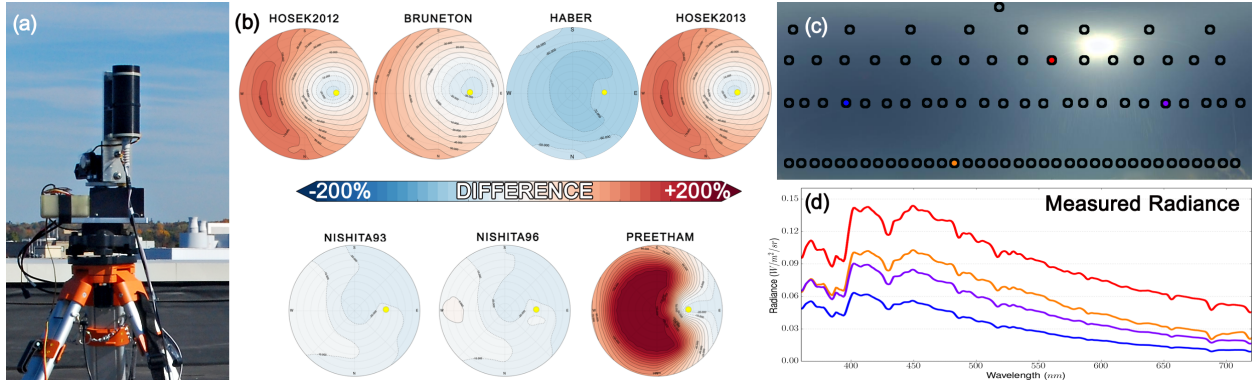


Figure 1: We capture the solar/skydome spectral radiance and compare state-of-the-art simulation models. (a) Our custom built solar-skydome scanner, (b) relative differences between state-of-the-art simulation models and our measured samples over the hemisphere, (c) example of sample points and captured sky imagery, and (d) spectral radiance curves for different sample points in (c).

Abstract

The illumination and appearance of the solar/skydome is critical for many applications in computer graphics, computer vision, and day-lighting studies. Unfortunately, physically accurate measurements of this rapidly changing illumination source are difficult to achieve, but necessary for the development of accurate physically-based sky illumination models and comparison studies of existing simulation models.

To obtain baseline data of this time-dependent anisotropic light source, we design a novel acquisition setup to simultaneously measure the comprehensive illumination properties. Our hardware design simultaneously acquires its spectral, spatial, and temporal information of the skydome. To achieve this goal, we use a custom built spectral radiance measurement scanner to measure the directional spectral radiance, a pyranometer to measure the irradiance of the entire hemisphere, and a camera to capture high-dynamic range imagery of the sky. The combination of these computer-controlled measurement devices provides a fast way to acquire accurate physical measurements of the solar/skydome. We use the results of our measurements to evaluate many of the strengths and weaknesses of several sun-sky simulation models. We also provide a measurement dataset of sky illumination data for various clear sky conditions and an interactive visualization tool for model comparison analysis available at <http://www.graphics.cornell.edu/resources/clearsky/>.

CR Categories: I.3.7 [Computing Methodologies]: Computer Graphics—Three-Dimensional Graphics and Realism;

Keywords: skylight models, measurements, validation, spectral

Links: [DL](#) [PDF](#) [WEB](#) [DATA](#)

1 Introduction

The sky’s highly varying appearance is critical for many applications. In the field of computer graphics, many sophisticated solar/skydome models have been developed primarily to create visually plausible images for the feature film and gaming segments of the entertainment industry [Sloup 2002]. Since the sky is certainly the most important light source for outdoor scenery, these models have also been used not only as backdrops, but as illumination sources to produce visually pleasing images. However, many of these existing skylight models target the creation of plausible images, but their physical accuracy has not been compared to measurements.

In contrast to the goals of generating beautiful imagery, other fields require dependable and accurate radiometric illumination. The computer vision field needs to know the qualities of the illumination source to accurately determine an object’s material properties under different lighting conditions. The design and analysis of the built environment require the accurate prediction of a building’s day-lighting behavior. The quality of natural daylight has been found to dramatically effect the perceived comfort of a building’s occupants and to improve patients’ recovery time. Two of the most important characteristics of light sources are their spectral distribution and their varying spatial-temporal radiance and luminance. Until now, despite much work in simulating the solar/skydome, capturing, measuring, and comparing the changing radiometric radiance of the solar/skydome has remained a substantial challenge. The absence of such data creates a need for an acquisition approach that precisely measures sky illumination.

Collecting radiometrically accurate measurements of the solar and

skydome illumination is a significant challenge. For this research, we develop a new system that simultaneously scans the sky and measures the spectral radiance, total irradiance, and captures high dynamic range (HDR) imagery. The resulting data is directly useful for comparing current skylight models by providing ground truth physical measurements. Several existing acquisition systems have focused on capturing the solar/skydome's irradiance or luminance. However, most previous approaches did not capture the spectral radiance distributions of the sky. This limits the applicability of the approaches since skylight radiances change very rapidly, both spectrally and directionally.

Our measurement data allows for a comprehensive comparison of several state-of-the-art skylight models with respect to the ground truth radiance and irradiance measurements. As an additional application which leverages the radiometric spectral data, we use the data to create a data-driven interpolated solar/skylight model which is useful for ground truth daylighting studies and provides more information than HDR photography.

Thus our contributions include:

- A multi-device acquisition technique for simultaneously acquiring the integrated solar/skydome radiance, the total irradiance of the hemisphere, and high dynamic range imagery of the sky. This includes the design of a novel solar/skydome spectral and spatial radiometric measurement scanner which is the fundamental technology for accurate sky measurements.
- A publicly available measurement dataset at 81 equal solid angles over the hemisphere available at <http://www.graphics.cornell.edu/resources/clearsky/>. This data is used to create a data-driven solar/skydome model.
- Comparisons of several state-of-the-art solar/sky model indicating their strengths and weaknesses, and graphically illustrating their deviations from measured results.
- An interactive visual interface depicting the appearance of the solar/skydome including spectral distribution, radiance, irradiance, and various error metric visualizations.

The availability of accurate measurements and an interactive visualization tool provides a framework for a comprehensive comparison analysis that can improve physically-based simulations of solar/skydome that better match the real world.

2 Previous Work

Both capturing the solar/skydome illumination, as well as modeling it, is a challenging multidisciplinary research problem. The problem is well studied in computer graphics, atmospheric science, and physics. While the sun is the most important light source in the sky, much of its light is scattered throughout the atmosphere before it reaches the surface. Accurate lighting models must account for both solar and sky dome contributions. Though skylight is often of secondary importance after direct sunlight, the sky is the main source of illumination during the early morning and evening hours. We recognize many existing sky models are concerned primarily with producing visually-plausible images for the movie and game industries. Although this restriction is acceptable for rendering, it is not acceptable for daylighting simulations where there is a large range of wavelength distributions. Radiance [Ward 1994] is one popular physically-based rendering tool that calculates daylighting factors, irradiance, and luminance that is widely used outside of graphics, namely in building design. We provide a strong experimental foundation that helps quantitatively ground the accuracy of these methods. A process to more robustly capture the skylight opens the door for future comparisons and daylighting studies.

Sky Capture Techniques. Many commercial systems for measuring various aspects of the sky have been developed, and are currently being used in meteorology and atmospheric science. They generally use a pyranometer [Abbot et al. 1916] to measure total hemisphere radiation which measures the global horizontal irradiance. These devices measure spectral distributions or sum wavelengths to produce one irradiance measurement. The pyranometer has a rotating disc that blocks the direct solar component to enable the measurement of the diffuse sky radiation. Common models include Kipp-and-Zoen and Apogee. A pyrheliometer measures the direct sun energy by pointing the device at the sun. The device typically has a narrow field of view to block non-solar light, and the device tracks the sun automatically throughout the day [Myers 2013]. A spot luminance meter [Zotti et al. 2007] measures the instantaneous luminance in the direction the device is pointed. Common models are available from Konica Minolta. Sky Radiometers measure direct solar radiation and diffuse sky radiation for 8-11 wavelength bands between 315nm to 2200nm. The most popular model is a Kipp Zonen POM-02. Stumpf et al. [2004] proposed a technique to directly capture the sky and sun by high dynamic range photography using a series of meticulously set aperture and shutter settings, however their approach has a limited spectral range.

Clear Skylight Models. One of the first simulation models used to describe luminance distributions in a clear sky was the Standard Clear Sky specified by the CIE (International Commission on Illumination). This model was originally intended to provide lighting designers with the ability to evaluate the luminance a building will receive. The model does not directly provide any spectral information, and the lack of color limited the model's utility for both rendering and daylighting design. The Perez All-Weather model [1993] presented a better analytic solution for simulating clear skies and the CIE [2004] modified and adapted Perez's formulation in their recent standard. The Perez and CIE equations adjust the luminance based on three non-intuitive and non-physical parameters. Perez [1993] suggested using tabulated values, and subsequently Preetham [1999] and his colleagues proposed solving the parameters analytically.

Rendering realistic sky color typically involves both single scattering [Nishita et al. 1993] and multiple scattering [Nishita et al. 1996] methods. Nishita and his colleagues proposed the first ground breaking work, which included color information, and they created one of the first plausible sky images useful for movies and games. They ignored spatially-varying ground interreflections and spatially varying particles in the atmosphere. Haber et al. [2005] further developed a multiple scattering model in a physically-based, brute-force numerical simulation of radiative transport in the sky. This model accounts for particles which vary spatially by altitude but not horizontally, which limits the model, for example, where smog above a city might locally skew atmospheric scattering in a given direction. Since, these brute-force simulation methods are computationally expensive, more recent techniques have been developed for approximating the clear sky. Several analytical models fit simulation data to the Perez Model equations rather than rely on tabulated data. These equations generally assume sky particle and scattering conditions are similar everywhere on the globe. Analytical methods such as the Preetham sky [1999], Hosek skydome [2012], and Hosek solar disc [2013] are extremely quick to compute, but these methods only approximate sky radiance.

Dobashi et al. first proposed a GPU-based method to simulate atmospheric scattering utilizing a spherical volumetric rendering approach. Hoffman and Preetham [2003] proposed simplified scattering equations to simulate the sky in real-time. This computation can further be accelerated by precomputing the atmospheric properties, such as transmittance and in-scattering, as a series of lookup tables which has been done by Bruneton et al. [2008] and Elek

and Kmoch [2010]. GPU methods create plausible sky images for games that run in real-time for games, but sacrifice accuracy for efficiency. All of the models described above are restricted to visible wavelengths and are primarily used for graphic renderings. To conduct accurate energy and daylighting studies for the sustainable design of the built environment, the full range of wavelengths must be considered, both spectrally and spatially.

The atmospheric science community also has a rich history of solving the radiative transfer equation for solar radiation simulations. Most of the spectral radiation models are computationally expensive to compute. Examples of some of these models include LOWTRAN [Kneizys et al. 1981], LibRadTran [Mayer and Kylling 2005], MODTRAN [Acharya et al. 2003], SBDART [Ricchiuzzi et al. 1998], and SMARTS [Gueymard 1995]. These models are highly regarded in the atmospheric science community for their physical simulation abilities. Atmospheric science models are generally concerned with precisely solving a single wavelength at a single angle. These models sacrifice speed for accuracy, making it extremely expensive to compute an entire solar/skydome image or rendering. Karayel et al. [1984] and Soler and Gopinathan [2000] looked at sky luminance distributions for daylighting calculations. This work differs from work from Tominaga et al. [2007] which attempts to extend RGB signals to hyperspectral from priors. Our measuring device takes ground truth data and does not infer the spectral distribution.

Skylight Comparison Studies. Zotti et al. [2007] provided comparisons between the sky luminance of the Preetham [Preetham et al. 1999] and CIE [Darula et al. 2002] skylight model and measurements taken by a Minolta LS-110 Luminance Meter. These measurements were taken by hand on a tripod by manually rotating the device. Their major insight demonstrated where the Preetham model produced poor luminance patterns compared to measured data. Luminance, however, does not measure or validate the electromagnetic radiation wavelengths of light. Building science researchers have recently addressed the problem of measuring and validating irradiance to various sky models [Diez-Mediavilla et al. 2005; Loutzenhiser et al. 2007; Noorian et al. 2008; Ochoa et al. 2011]. These comparisons, however, only focus on total or diffuse irradiance and do not consider any directional radiance measurement or validation studies. Most Building Simulation studies [Grynberg 1989] also focus on comparing measured results to sky models simulated in Radiance [Ward 1994]. Additional luminance and irradiance measurements and comparisons were done by Littlefair [1994] and Ineichen et al. [1994] which focused again on the CIE and Perez models.

3 Framework Overview

The goal of our framework is to provide a comprehensive method for measuring the solar/skydome that is applicable for experimentally comparing current state-of-the-art sky models. The sky capture process measures radiance, irradiance, and captures high dynamic range images of the skydome. The comparison stage uses the measurements to determine the accuracy of various state-of-the-art solar/skydome models. We developed a tool to help analyze and visualize the various strengths and weakness of all the solar/skydome models. Additionally, we further utilize the data to produce a fully data-driven spectral skylight model for daylighting studies at particular capture times.

Data Acquisition Design. The purpose of the data measurement acquisition setup is to capture the solar/skydome’s spectral illumination. Our measurement process is divided into three stages: radiance measurements, irradiance measurements, and HDR-images. Figure 2 illustrates the three devices we use: a custom-built sky ra-

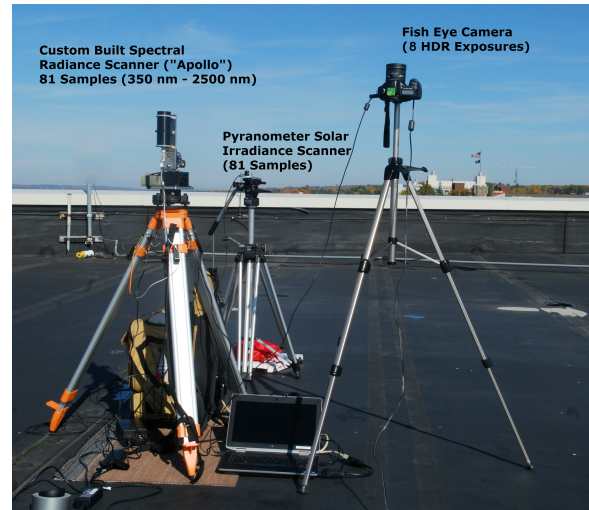


Figure 2: The measurement setup we use to capture skylight. The custom-built radiance scanner (left) captures spectral samples of the sky. The pyranometer (middle) samples the irradiance of the skydome, and the Canon camera (right) captures HDR-images.

diance scanner, a pyranometer to capture irradiance, and a Canon 5D with a fisheye lens to capture HDR-imagery. Section 4 details the structure and basic operation of what hardware we use, what data we capture, and how we store the data. For the first time this dataset allows more accurate spectral comparisons of skylight. This collection of measurements becomes our sky appearance database.

Comparison Analysis. We compare the measured data and the output of several state-of-the-art solar/skylight models in Section 5. We selected seven different approaches which contain: six skylight models: the Nishita single scattering Model [1993], the Nishita multiple scattering Model [1996], the Preetham Model [1999], the Haber Model [2005], the Bruneton Model [2008], the Hosek Skydome Model [2012], and three solar models: the Preetham Solar Model [1999], the Bruneton Solar Model [2008], and the Hosek Solar Radiance Model [2013] to analyze. We compared the radiance (Section 5.1), irradiance (Section 5.2), and illumination (Section 5.3) of the various models. Section 7 provides insights we found while comparing the strengths and weaknesses of the various models, and describes when to use each approach.

Data-driven Skylight Model. One application of the measured spectral radiance data is the creation of a data-driven spectral sky model. Normally, data-driven sky models only use HDR-imagery [Stumpfel et al. 2004]. However, this method is limited only to RGB and does not provide spectral varying data needed to illuminate spectrally varying BRDF, spectral varying phase functions, and daylighting studies. We introduce a new data-driven method for synthesizing spectral sky illumination. We spherically interpolate the discretized measured radiance samples from our custom-built sky scanning device. Section 6 describes the details for creating this spectral data-driven sky model.

3.1 Color Renderings and Tone Mapping

For visual comparisons written in this paper, we render and tonemap the images in sRGB. We render all images spectrally between 350nm to 830nm with 40 spectral bins. We convert these images to CIE XYZ space and mapped them to sRGB. We use the Reinhard et al. [2002] technique followed by gamma correction to tonemap recorded radiance values to the low dynamic range

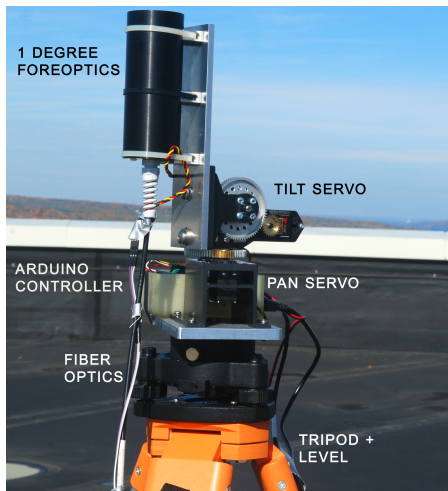


Figure 3: The custom-built radiance scanner which captures spectral samples of the sky. The device features interchangeable fore-optics lenses which send the light to a spectroradiometer which measures the spectral radiance between 350nm to 2500nm. The device is rotated to any angle by an arduino which controls 2 servo motors.

displayable for the paper. Please view the paper's images on a color calibrated monitor. In the supplementary material, we provide high-dynamic range EXR files so the reader can view the full dynamic range of some of the results.

4 Data Acquisition Design

The important properties of daylight motivate the need to meticulously capture the spectral radiance, irradiance, and HDR imagery of the entire sky. We design a unique multi-device acquisition system to capture these features.

4.1 Spectral Radiance Measurements

To measure radiance our setup incorporates a spectroradiometer, which is rotated and tilted, with a single fore-optics lens and a fiber optic cable. Figure 3 shows a photograph of this sky-scanning radiance instrument. Spectroradiometers are the most accurate measuring devices for capturing the spectral energy distribution of any light source. We utilized an ASD Fieldspec Pro Hi-Res spectroradiometer for the spectral data collection. The device measures a spectral range from 350nm to 2500nm which includes some ultraviolet, some near infrared, and all of the visible spectrum wavelengths. The device scans at roughly a 1.4nm wavelength resolution in the visible range, and 3nm in the near infrared. The device is fitted with either one-degree or eight-degree fore-optics which subtends the field-of-view by capturing the light through the fore-optics down the fiber-optics. Most of the scans in our measurement database use the one degree fore-optics, but some scans include the eight degree fore-optics (One and eight-degree fore-optics were the two light collimators we had easily available. The spectroradiometer could be fitted with custom designed fore-optics if desired.)

Each measurement sample contains the spectral distribution (nm) and the radiances. The measured radiance values have units of power (W) per unit area (m^{-2}) per steradian (sr^{-1}) per unit wavelength (nm^{-1}). Figure 4(a) shows a radiance measurement's sample spectral distribution varying spatially across the sky. Figure 4(b) shows the same measurement angle sampled every 10 minutes for

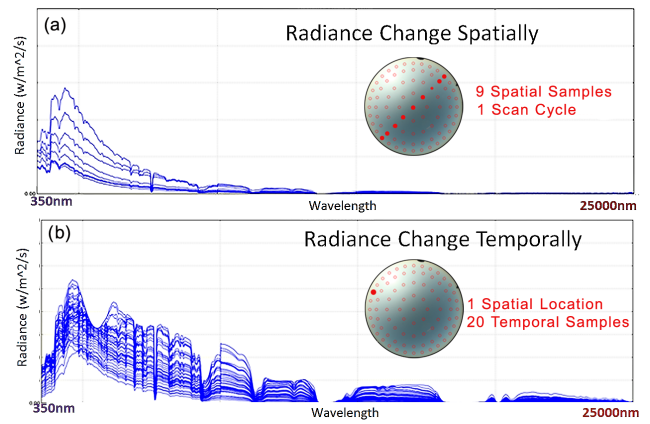


Figure 4: (a) shows the measured output of the sky showing spatial variance of skylight with 9 spatial samples for one scan cycle, and (b) shows the temporal variance of skylight by showing how the spectral distribution changes for one spatial locations over 15 minute scan cycles.

a few hours. These measurement readings illustrates how the sky's spatial and temporal spectral distribution changes over the hemisphere and throughout the day.

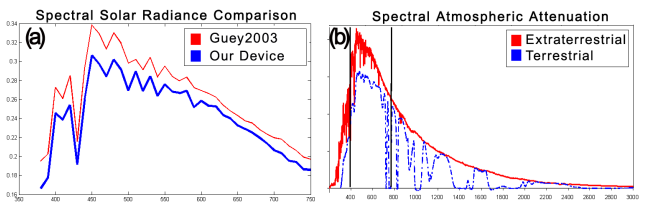


Figure 5: This image demonstrates the general accuracy of the measurement device. (a) NASA solar radiance data - taken from Guey et al. (2003) (red) is plotted against our measurement (blue). The measurement is what we expect since light is attenuated through the atmosphere. (b) A published graphic that shows this effect by a satellite above the atmosphere.

For each vector direction, the device takes 10 samples and averages the data to reduce measurement noise per measured wavelength. At the end of a full sky scan, we measure the dark current to further reduce noise in the spectroradiometer measurements ensuring more accurate data. Figure 5 (a) demonstrates the accuracy of the device itself - a spectral sample of the sun plotted against tabulated data obtained from NASA (measured at the top of the atmosphere.) Our measured graph is slightly lower since light is attenuated through the atmosphere as it reaches the Earth's surface, and passes through different absorption bands. This follows other published data Figure 5 (b) which demonstrates this effect. Our measurements are repeatable across different measurement days and return the natural variation you would expect to find from different sky conditions.

Our device uses two servo-motors to pan and tilt the device's fore-optics to scan the sky. The motors are controlled by an Arduino controller which accepts a pan and tilt angle to move the device. These motors are accurate and repeatable. The rotational error of these devices is around 0.5 degrees. This is sufficiently accurate to capture skylight since the motors move the fore-optics to any position to scan the skydome. The device takes around three minutes to sample the entire hemisphere at 81 sample points. We noticed that spectral distribution measurements were more sensitive to elevation errors than to azimuthal errors.

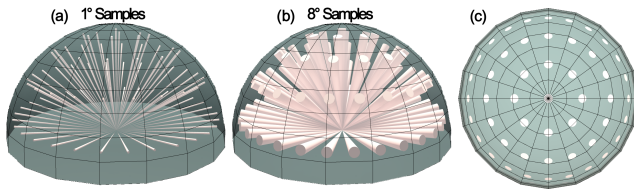


Figure 6: The sky-scanner uses different fore-optics to scan the sky. We choose a pattern to scan 81 equal solid angles. The left image shows coverage at 1 degree fore-optics, the middle image shows 8-degree fore-optics, and the right image shows the plan view coverage of sample coverage on the hemisphere.

We can program any custom scanning pattern to sample the skylight in the skydome. We selected a pattern based on the approach by Shirley and Chiu [1997] to divide the hemisphere into samples of equal solid angle, or equal area on the unit hemisphere. (We use the source to code for this concentric mapping directly from the Shirley-Chiu paper). The samples are evenly distributed across the sky, are symmetric from the zenith, and do not overlap due to the subtended angle of the fore-optics. Figure 6 illustrates the sampling pattern and fore-optics we used in our scans. Any pattern may be programmed and scanned by the device, including the one proposed by the CIE [1994]. Once a sampling pattern is devised, the pattern is sent to the device as an array of angles. Care must be taken to ensure the fiber optics do not become twisted or tangled during the scanning procedure. Therefore at each elevation we unwind the pattern to ensure the fiber optic cable is not bent.

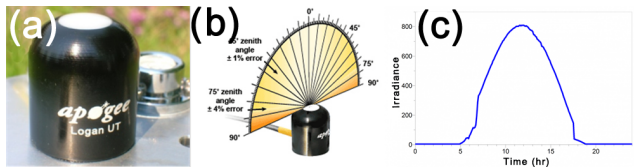


Figure 7: This image provides details of our pyranometer which measures the irradiance. (a) Shows the device we use: an Apogee pyranometer to measure the total irradiance, (b) Shows the cosine response of the device, (c) Shows sample data captured by the pyranometer for a typical clear day.

4.2 Irradiance Measurements

We use an Apogee pyranometer to measure the total hemisphere irradiance (W/m^2), also known as the global shortwave solar radiation (Figure 7(a)). The pyranometer has a 180 degree field of view which measures light from the entire skydome. Figure 7(b) illustrates the cosine response for the device. Specifically, we use a silicon-cell pyranometer manufactured by Apogee with a diffuser. For our Apogee sensor, a conversion factor of $0.5 W/(m^2 * mV)$ is used to convert the sensor output to the final radiation value. The conversion factor is based on the output sensor voltage which is different per device. For our pyranometer the sensor output is $2.2V$, and the device is calibrated such that:

$$2.2 * ConversionFactor = DirectSunlight * \frac{W}{m^2} \quad (1)$$

The conversion factor from Equation 1 simply scales the raw output to irradiance. The device is wired to the Arduino controller and samples the irradiance once every time the sky-scanner takes radiance measurements. The voltage signal of the sensor is converted to radiation incident on a horizontal planar surface since the signal is exactly proportional. The sensor is calibrated directly to a clear

sky conditions. Figure 7(c) provides sample output from the device over a clear day. The values are averaged and accumulated to determine the final total irradiance measured during the scan. We take a value every sample in case the sun is partially occluded and drastically changes the total irradiance, and thus we can account for any noise in the samples during the radiance scan.

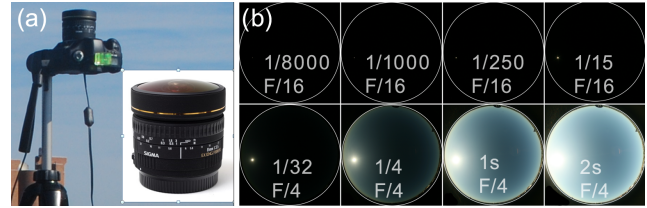


Figure 8: This image provides details of our HDR imagery setup. (a) We use a Canon 5D camera with a 8mm fish-eye lens to acquire 8 photographs (b) which capture the wide dynamic range of the sky.

4.3 High Dynamic Range Imagery

To capture HDR imagery of the sun and sky, we follow the method outlined by Stumpf et. al [2004]. This method uses a Canon full-frame camera (5D), a fisheye lens (Sigma 8mm), a neutral density filter (Kodak Wratten 2 ND 3.0), and a laptop (Figure 8(a)). On a clear day, varying exposure times and aperture settings captures the full 17 stop dynamic range of the sky with eight photographs. Figure 8(b) shows the HDR sequence and camera settings which follow Stumpf's approach. The first four images (top) the solar disc, and the last four (bottom) capture the diffuse skylight. We use the library *libphoto* which allowed us to tether the camera to a laptop and automatically capture and download the HDR sequence. The HDR sequence takes approximately 40 seconds to capture. The HDR images are useful to visualize the current sky conditions. We provide the RAW images captured; but the lens distortion, chromatic aberration, vignetting, and neutral density filter must be accounted for to produce a properly calibrated HDR stack.

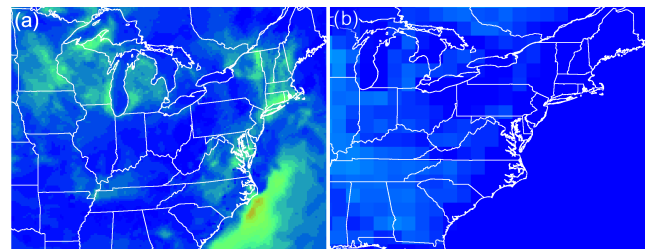


Figure 9: This image visualizes weather data. (a) shows the visibility data for the East Coast. (b) shows the ground albedo.

4.4 Atmospheric Weather Data

Weather data provides detailed classification of prevalent atmospheric conditions at the measurement location. Atmospheric conditions contain complex structure and aerosol changes. We used three sources of data to qualify the current sky. **Rapid Refresh** (RAP) assimilates data from ground based radar, conventional weather stations, and satellite data. This data, in Figure 9, provides 2D grids for visibility and albedo (<http://rapidrefresh.noaa.gov/>). RAP also provides 13km 3D grids for a wide range of atmospheric conditions which include: temperature, pressure, and humidity. This data is updated hourly. **SYNOP** and **METAR** are two ground-based conventional weather observation points made by manned and automated weather stations, usually around airports. These

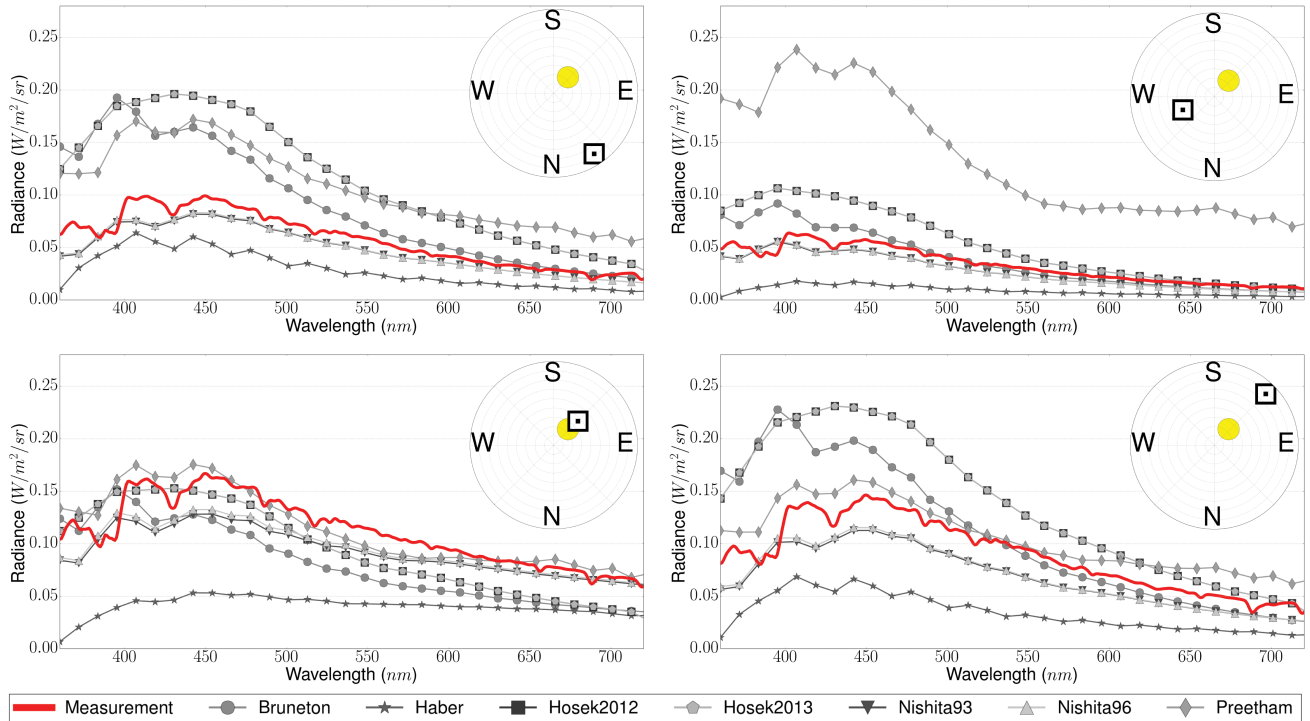


Figure 10: Left: This figure shows the spectral difference of radiance between measured data and 7 state-of-the-art solar/skydome models for four spatial angles. The measured radiance ($W/m^2/sr$) is shown in red.

also provide measures of visibility and sky clearness. SYNOP is updated every six hours, and METAR is updated every hour.

Care must be taken to ensure that visibility reported by RAP is consistent with turbidity defined by Preetham and Hosek. Here turbidity measures the aerosol content of the air. The following equation converts the value to the expected turbidity term:

$$turbidity = 2^{(-2.3 * \log(0.26 * \frac{\log_{10}(visibility+0.5)}{\log_{10}(4)}))} \quad (2)$$

4.5 Solar/Skydome Measurement Dataset

From the measurements taken with our device, we then create an accurate measurement dataset for the community. The result is the acquisition of a hemispherical illumination source defined by a wavelength based radiance across the entire skydome. These measurements define the sky's illumination. We have captured many samples of clear sky data from a variety of different spring, summer, and fall days. The data is organized where each time-slice exists in a folder with the capture time in GMT as its name. The folder contains two text files for the radiance and irradiance, and the eight HDR photographs for that scan cycle. We also include a method to gather the weather data to explicitly classify current sky conditions. This dataset allows more accurate spectral comparisons of skylight against various simulated models. The data is captured simultaneously for every time-slice. The data itself is provided in raw format and not integrated until the data is used in various applications.

5 Comparison Analysis

Over the past twenty years, various skylight models of increasing complexity have been proposed. We select seven frequently used

and cited solar/skydome models and compare the radiance, irradiance, and visualization of the resultant illumination for each. Six of these seven publications propose skydome models, and three include solar models. The skydome models we compare are the Nishita et al. [1993] single scattering Model, the Nishita et al. [1996] multiple scattering Model, the Preetham Model [1999], the Haber Model [2005], the Bruneton Model [2008], the Hosek Skydome Model [2012]. The three solar models are the Preetham Model [1999], the Bruneton Model [2008], the Hosek Solar Radiance Model [2013].

We develop and present an interactive interface tool which can load any sky model's radiance, irradiance, and imagery data for the skydome hemisphere. We have open sourced this tool so other researchers can run similar comparisons. Though we only choose 7 models to compare, any model can be easily loaded under this tool. The graphic interface features a wide range of comparison tools that compared the different model's strengths and weaknesses when compared to our measured data. We plot a variety of data, difference information, and imagery.

The solar/skylight models are all implemented in the Mitsuba framework [Jakob 2010] to ensure the comparison analysis experiment is consistent. Most models are formulated on a wavelength basis and were run spectrally. Model comparisons span a spectral distribution between 360nm to 830nm with 40 spectral bins. Our results only show data between 360nm to 720 nm since some models do not have data beyond that range. We use this spectral range since most skylight models were primarily designed for the visible range to make images. To run the models spectrally, we use the same solar table, and the same Rayleigh, and Mie constants across all models. We replaced the RGB triplets for these constants with discretized spectra between 360nm and 830nm in 5nm bins. These spectra were interpolated and sampled at each of the 40 bins. We simulate all models with the same parameters (when applicable in

the model), such as turbidity and ground albedo. The turbidity for the clear sky was found from the closest weather station for that day. Wherever possible, we directly integrate the author's source code into their own Mitsuba plug-ins [Preetham et al. 1999; Bruneton and Neyret 2008; Hosek and Wilkie 2012; Hosek and Wilkie 2013]. The other models ([Nishita et al. 1993; Nishita et al. 1996; Haber et al. 2005] were carefully implemented from their respective papers to the best of our ability. Additional simulation data can be easily added both to Mitsuba and to the interactive framework.

The choice of parameters used to drive the analytical models and the path traced models is derived explicitly from the measured data discussed in Section 4.4. Rapid Refresh data provides color and intensity for the current ground albedo, and we use Equation 2 to derive the turbidity. This data also explicitly drives the inputs for the Haber model. We feed the humidity, per layer, into OPAC [Hess et al. 1998], which is used by Haber's model.

5.1 Spectral Radiance Comparisons

We compare the spectral radiance in two groups: six skydome models and three solar light models. For the skydome radiance comparison we use time-slices where the solar disc did not cross one of the 81 measured points. For the solar light comparison, we directly measure the solar region with the sky scanner and compare the solar model simulation data at that specific angle. This ensured that we are only comparing skydome to skydomes and solar region to solar region. (Our device scans the entire solar/skydome. This grouping was only done to consistently compare various simulation models.)

Figure 10 plots the spectral radiance of the six skylight models with the measured data from the spectral sky-scanner for a four different angles. We graph absolute radiance at each wavelength. In the supplementary material, we provide a complete and detailed analysis of the skydome for all 81 sample points for a few timeslices. We provide other visualizations of the differences. We calculate the R^2 difference between the sample points per wavelength and the measured data, the total R^2 difference summed over wavelengths, and the relative difference. Figure 11 plots the spectral radiance of the three solar models with the measured solar data.

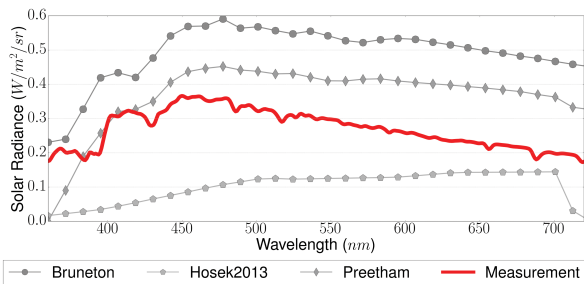


Figure 11: This figure shows the spectral plots of radiance between measured data and the 3 state-of-the-art solar models for one scan cycle. The measured radiance is shown in red.

5.2 Irradiance Comparisons

We calculate the total irradiance from the seven solar/skylight models. Here we made an assumption about combining the solar/skydome models. We added the Preetham solar model to every model except the Bruneton2008 and Hosek2013 models. Those models use their respective solar models and skydomes. Up until the publication of the Hosek2013 solar model, this was an acceptable practice in many renderers. This combination exists in Mitsuba, V-Ray, and other popular renderers as a default solar/skydome

model. The evaluation results are summarized in Figure 12 in which we compare a five hour block (20 different measurements) of clear sky conditions. We compare the total irradiance simulated to the total irradiance measured by the pyranometer. These graphs capture how the models perform over all the angles in the hemisphere. We compare the measurements to the pyranometer since the spectroradiometer only samples discretized points and not the whole sky, and the HDR-imagery texel size varies across the image. The pyranometer provides an effective way to measure the irradiance without having to discretize the integration across the hemisphere from the other measuring techniques.

Figure 12 shows that the Hosek solar model and the Bruneton solar/skydome produce an unnatural bump in irradiance at high solar angles. This was a surprising result. The Hosek skydome (with the Preetham solar model) significantly corrected the sky's irradiance compared to the Preetham skydome. The two Nishita models tend to best follow the measured irradiance curves.

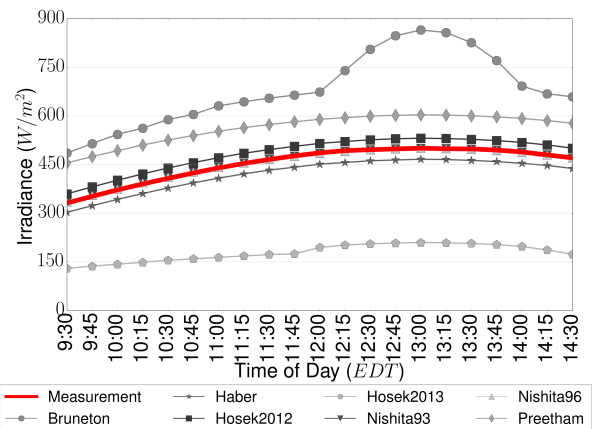


Figure 12: This figure shows the difference of total irradiance between measured data and 7 skylight models for part of the day. (We provide a comparison of full day irradiance in the supplementary documentation.)

5.3 Illumination Comparisons

Many graphics applications need scenes lit by these solar/skydome models to produce physically accurate renderings. We rendered fisheye views of all the skydomes and compared them to tone-mapped HDR-imagery in Figure 13 using the tone mapping approach discussed in Section 3.1. This figure shows the seven solar/skydome models at four different times of day on May 26 and 27, 2013 in the United States. This result provides a visualization of how the illumination color varies between the different models over various times of a day. In the supplementary material, we provide more time comparisons of the color differences of the various models and a dynamic sequence over a whole day. The change in color occurs due to the different methods each simulation uses to simulate the skydome.

In Figure 18(top), we illuminated a kitchen scene with a few of the solar/skydome models. This demonstrates the impact the different models have on indoor scenes. Both the colors and intensity vary throughout the day between the models. This is potentially important for situations where the color and appearance of objects matter. The final illumination could vary depending on which model is used. Figure 18(bottom) show the luminance and intensity curves commonly used in daylighting studies.

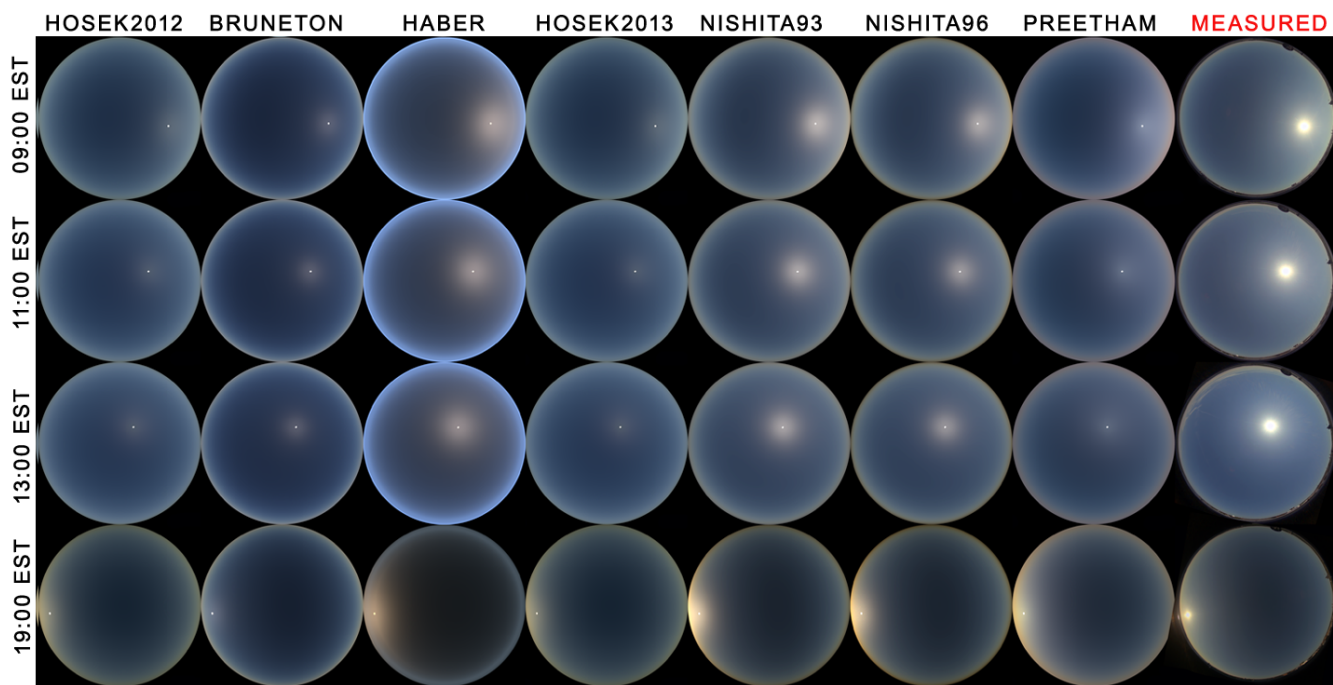


Figure 13: This image shows the seven simulation models compared with their tone-mapped fisheye images. (Note: The fisheye images use the same tone-mapping technique as the simulation figures.)

6 Data-Driven Spectral Skylight

Using the method for capturing spectral radiance data described above, we are able to reconstruct realistic spectral illumination for outdoor scenes across the entire visual spectrum, and not only RGB. We start by projecting the 81 measured data points with positions represented in spherical coordinates onto the unit hemisphere. Bicubic spherical interpolation is used to reconstruct radiance values for positions on the hemisphere that lie in between measured radiance samples. For the solar disc, we sample the sun directly in our capture process, and use that spectral information to drive the solar model directly. Depending on the user’s requirements, the sky can be sampled with any pattern providing even better results. This model produces more accurate spectral information than HDR-imagery.

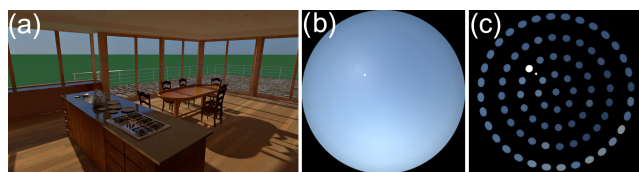


Figure 14: This image shows the results of our data-driven spectral skylight. (A) shows a scene illuminated with the data driven skylight shown as a fisheye image in (B). (C) shows the samples points and their corresponding RGB color.

A CIE XYZ fitting can also be done for applications where the full spectral model is not needed. Figure 14 shows a sample scene with the illumination derived from the data-driven method. Figure 14(B) shows a fisheye view of the constructed skydome in sRGB. Figure 14(C) shows the conversion of just the sample point themselves. This approach provides full spectral data for illumination which could be used for spectrally varying BSDFs, daylighting, and thermal studies that could not be simulated directly with Stumpfel et al. [2004] proposed technique. Daylighting studies specifically

can take advantage of having a fully spectral sky. The data-driven model differs from HDR-imagery techniques since it explicitly provides the full spectral sky. HDR-imagery [Debevec 1998; Inanici and Galvin 2004] tries to use machine learning to predict the spectral radiance, but does not provide explicit measurements. The measurements provide the exact radiance at a particular angle and does not worry about an HDR camera’s response curve and lens issues (chromatic aberration, distortion, vignetting, etc.)

7 Discussion

We have presented a unique method to capture the physical daylight of the solar/skydome. By using our custom-built sky-scanning device, we gather ground-truth data that measures incoming light spectrally, spatially, and temporally. Our analysis of the captured data currently only considers clear sky days without any clouds. We choose to omit cloudy skies from this study due to the rapid atmospheric changes that clouds produce and limitations associated with our capture method. More precisely, our sky-scanning device takes three minutes to scan and capture the entire skydome. While this length of time is insignificant for the gradual atmospheric changes on clear sky days, the presence of clouds introduces rapid changes to the atmosphere that prevent consistent measurements across the full skydome.

We provide a comparison of current state-of-the-art solar/skydome simulation methods with our ground-truth data scanned by our approach. Analyzing these comparisons show interesting insights in the current state-of-the-art of sky rendering. Analytical models are optimized to satisfy speed and ease of rendering while minimizing any expensive path-tracing steps. The seed images for the non-linear optimization step are path traced, usually at a single location, but simplify down to a few formulas for generalized rendering. Through comparisons to our measured data, we show that most analytical models produce plausible results but vary significantly in various regions of the skydome.

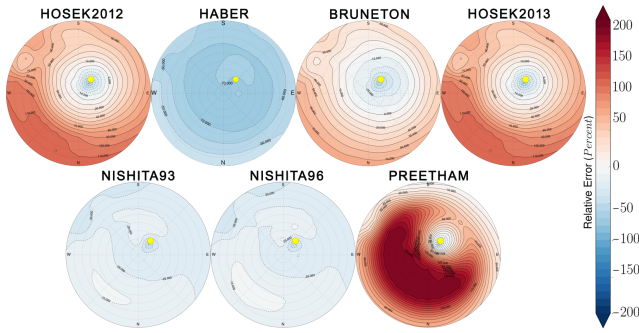


Figure 15: This figure plots the radiance difference over the skydome. We have interpolated the difference between the measurement and simulation for this visualization to better illustrate where the models differ.

It should be noted that our comparison methodology of measurements to the various sky models is driven from the best data we were able to find, however it is difficult to remote sense the exact atmospheric conditions at a particular time. 3D aerosol distribution data is not currently accurate enough to drive a highly authoritative reference simulation. RapidRefresh data only provides 13km regions which blur the aerosol distributions and does not provide the required granularity for accurate atmospheric composition data for the measurement locations. In the past, this granularity was not needed and our work demonstrates a clear need to have fine-grained altitude dependent variability of 3D aerosol distributions.

The major differences between the measurement data and most of the simulation models occur around two regions. The first major difference region is located around the current position of the solar disc. Figure 15 plots the relative radiance error (summed equally across all wavelengths and interpolated over the skydome). This graph illustrates how the difference is significant near the solar disc. Specifically, the models undershoot the radiance in this region. The second major difference region is the area near the horizon. A variety of the models produce vastly different spectral distributions around the horizon (Nishita single scattering and Preetham). Visually these models have a red saturation around this region which the Hosek skydome fixed for high solar angles. Figure 15 percentage difference plots would improve by driving the initial simulations with better 3D aerosol distribution data and this should be considered when viewing these plots.

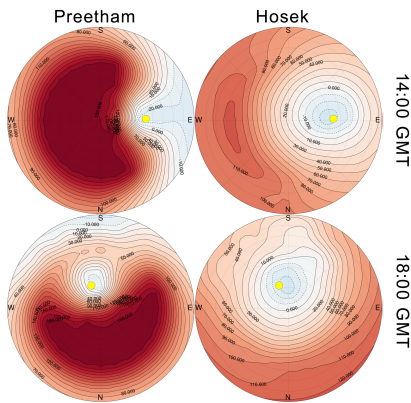


Figure 16: This image directly shows the total radiance error plots for the Preetham and Hosek skydome. This figure illustrates how the Hosek skydome significantly improved the Preetham model across a large portion of the skydome.

Our comparisons also demonstrate how and where the Hosek skydome improved the Preetham model both spatially and spectrally. Since we have a ground-truth data-set, we are able to quantify improvements. Figure 16 illustrates this difference and highlights specific areas of improvement for the Hosek skydome. The error plots show how much better the Hosek model performs.

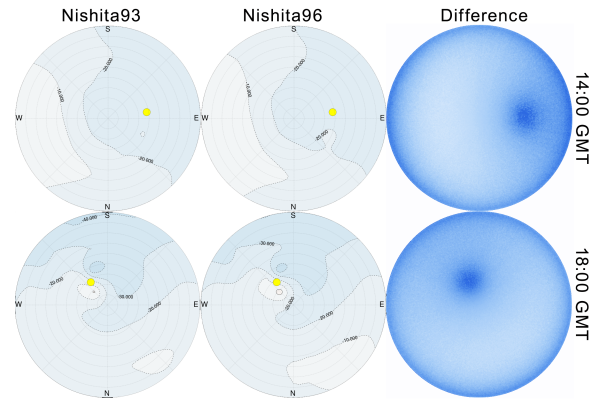


Figure 17: This image shows total radiance error graphs for both the Nishita single scattering Model and the Nishita multiple scattering Model. We also provide the difference image (between single and multiple scattering), where the areas in dark blue show the primary areas where multiple scattering has a direct effect.

Our data reinforces the importance and accuracy improvements associated with using a fully path-trace-based method when rendering the solar/skydome. The path-traced models more accurately predict the scattering effects at a particular point in time. Examples of this are the path-traced methods of Nishita et al. [1993] and Nishita et al. [1996]. The Hosek model is also initially brute force path traced, it is important that the atmospheric layering and composition used for the reference simulations are similar. Our comparisons have only analyzed the analytical results of the Hosek model, however reinitializing the model with new path traced results with the exact atmospheric conditions should change the model's accuracy. Furthermore, the importance of the multiple scattering from Nishita [1996] increases as the solar elevation decreases due to the increased amount of the atmospheric light rays must traverse. At high solar elevations on clear days, single scattering dominates. In addition, as atmospheric turbidity increases, the effects of multiple scattering are more pronounced. This follows the results of Bary and Eshelbach [1974] who studied the ratios of primary scattering to total scattering of sky radiance. Figure 17 illustrates where multiple scattering has a direct effect on the skydome.

The difference between the measurements and models occurs for a variety of reasons. The majority of the models assume aerosol properties are constant at every location (Haber is the only model to account for aerosol changes, but only in layers). Aerosols are not constant in the atmosphere, especially for cities such as Los Angeles and Shanghai, where dense areas of particles in the air show the anisotropic nature of atmospheric conditions which vary both vertically and horizontally at a fine scale. Additionally, the distribution of haze in the lower atmosphere is typically fairly different across climate zones. Some models also assume you are at ground level, so it becomes harder to accurately simulate a sky in a city such as Denver, CO (which is one mile above sea level). There is also a unique impact of light's attenuation per global position. All the models account for the sun location change since all allow the latitude and longitude to account for the proper solar position, but not the change in the cycle of the sun's power. Many of the models also approximate Mie scattering by using a Henyey-Greenstein scattering function. These functions are poor approx-

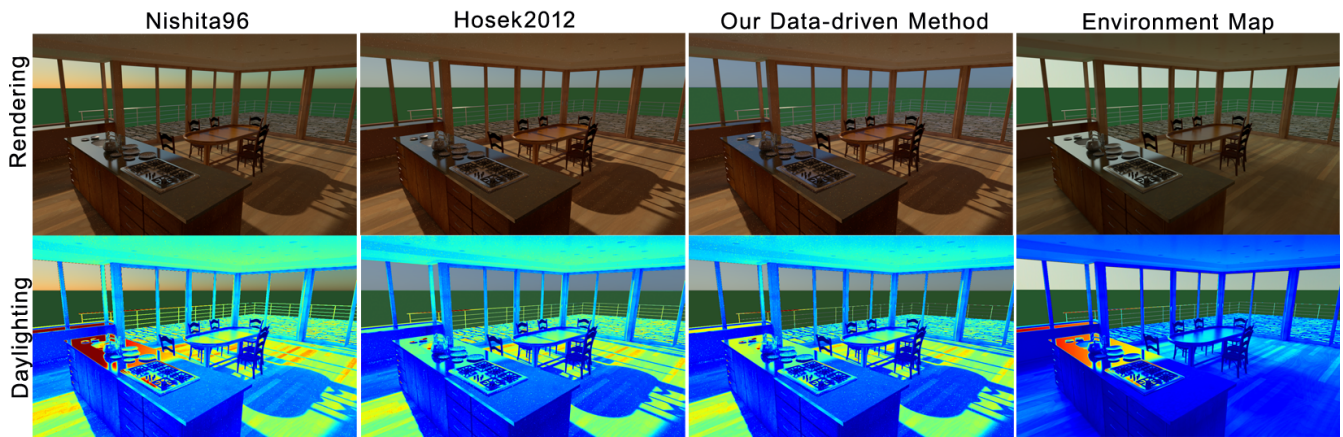


Figure 18: The *top* row shows the results of lighting a test kitchen scene with various models. The *bottom* row shows the differing daylight illumination between the various models. The times are shown in GMT for a location on the East coast.

imations for atmospheric scattering as turbidity increases. In our simulations, we drove the Haber model two ways: from synthetic data which assumed a data inspired starting point and an exponential falloff for atmospheric properties, such as humidity, and directly from RapidRefresh data which explicitly defined those properties per layer for the given time-slice. The RapidRefresh data driven approach tended to underestimate the radiance, while the synthetic data overshoots. We noticed that properties such as humidity did not exhibit a linear falloff in measurements and many layers had little to no humidity on clear days. (In the supplemental document, we provide a side-by-side illustration of the Haber model using both techniques).

We manually tested the choice of parameters by hand to see if there was a better fit to the measured data. Specifically, this was done by adjusting the inputs for the Haber model and the Hosek skydome. For the Haber Model, we tried both the exponential falloffs and varying the atmospheric properties. For the Hosek skydome, we discretized ten turbidities by ten ground albedos and ran 100 simulations. This manual search through the space did not produce better fits to the measured data.

After analyzing the data, we evaluated the different simulation models’ strengths and weaknesses. The Nishita models are excellent in accounting for the direct solar and scattering parameters since they in essence run a brute force path-trace on the scene. The major concern is that brute force path trace is not applicable for real-time applications. The Haber model is designed for more plausible sunrise and sunset images since the model accounts for twilight phenomena, but significantly underestimates the radiance at other times of day. The model accounts for optical changes in the density of the atmospheric layers which we drive directly from RapidRefresh data. Haber, however, also requires a brute force path-trace which is slow. If execution time is not a constraint, path-traced models will produce the best results. The analytic models (Hosek and Preetham) and the Bruneton real-time model produce very fast results which balance accuracy with usability. Preetham had an unnatural spectral distribution near the horizon that the Hosek skydome corrected to produce much more natural and realistic looking images. Hosek also performs better spectrally. These models should be used when speed is a major concern.

To amplify the importance of physically correct solar/skydome illumination models, we illustrate their impact on daylighting studies for a known kitchen environment. Figure 18(bottom) illustrates this daylighting study and how the various models produce differ-

ent results. This is important for accurate physical modeling, but necessary for building code compliance with respect to luminance on pre-defined surfaces.

Since our approach measures all light incident on our sensor, we measure the light from the current atmospheric conditions. We currently do not measure skylight polarization. Polarization influences the appearance of reflections with highly specular surfaces [Wilkie et al. 2004]. Stumpfel [2004] provides a simple technique to begin to quantify this parameter with HDR-imagery, and Pust et al. [2007] suggests a more accurate technique using liquid crystal variable retarders. As more simulations, renderers, and BRDFs support polarization, this would be an interesting feature to measure next.

8 Conclusions and Future Work

We present an acquisition approach for capturing the physical illumination of the sun and skydome. We also provide a dataset of sky measurements from different clear sky conditions from various times and days during the spring, summer, and fall. Currently this dataset has over 100 samples. The approach captures the spectral radiance, irradiance, and HDR imagery of the sun and skydome. The data we capture is useful for comparing the strengths and weakness of various models, and we use it to conduct a comparison of seven solar/skydome models. We plan to release both the skylight dataset and the visual interface to the community. Additionally, we use the capture data to produce a spectral data-driven sky model constructed from the measured samples. The resultant illumination model can be used for rendering, daylighting studies, or thermal evaluation since the illumination information spans a wider spectral range of 350nm to 2500nm, as opposed to an HDR image.

We chose to focus on building a system to capture spectral and spatial data for a given solar/skydome. We further compared and validated many assumptions and theories made over the last 25 years of sky rendering research. A natural extension is to investigate whether our data can be combined with current analytical and path tracing methods to increase their accuracy, specifically in areas where they generally differ significantly from measurements. Finally, an exciting area for future work is to create a new sky rendering technique that is directly inspired from the captured sky radiance data. The data we capture provides a much greater radiance spectrum than previously simulated in common computer graphics applications, and additionally provides accurate ground-truth measurements to drive this model. This would open new opportunities to conduct spectrally accurate daylighting and energy studies that

would not otherwise be possible.

In the future, we hope to leverage the information we learned from the measurement data to produce a more accurate solar/skydome simulation model, which reproduces a variety of sky conditions. The acquisition approach provides novel insights towards where to focus future attention. In the current models, the region around the solar disc tends to differ most significantly from actual measurements. This area is where the rates of change, both spectrally and with respect to the magnitudes of the radiance are greatest. Another area of interest is the at low azimuth angles near the horizon where spectral and radiance values differ significantly from our measured data. This area also tends to disagree with our measured data. This happens for several reasons: either the aerosols in the atmosphere are not being accurately accounted for, or the Henyey-Greenstein scattering approximations are not robust enough to capture these unique Mie scattering effects.

While we propose one possible scanning configuration, our system could be improved by customizing the scan pattern to fit the specific need of an application. For example, the CIE has set various sky sampling patterns for luminance distributions. These same patterns could be programmed into our device. The device is limited to scanning a narrow field radiance of either one or eight degrees. One could attempt to use other fore-optic lenses to perform the different scans of the sky radiance. Additionally, a spectral pyranometer could be used to compare the spectral irradiance output of various solar/skydome models. Though our data currently only contains one geographical location, we hope to scan different regions in the near future.

A current limitation of the scanning device deals with the spectroradiometer. The device itself was not designed explicitly to capture skylight, therefore the spectroradiometer has trouble capturing accurate measurements at early dawn and dusk. There is not enough light for the device to operate reliably. The shutter time is constrained, and increasing the shutter time subsequently increases the total scan time for the sky. Furthermore, the scanning of light at dusk and dawn needs to be faster, not slower. Dusk and dawn have the most dramatic and quickest changes, particularly with respect to the spectral distribution of the sky. We used an ASD Fieldspec Pro (which is around 10 years old). A newer spectroradiometer with faster speeds and sensitivity would alleviate this limitation. Another limitation we face is finding fine-grained 3D altitude dependent aerosol distributions better than the RapidRefresh data.

Our capture approach is a straightforward way to directly provide a basis for comparing various skylight models. Since these skylight models are used in a variety of applications, it is important to compare the accuracy of these models. In the future, we plan to capture a wider range of sky conditions to compare and validate. This would be useful for conducting a similar study for all the sky illumination models under all-weather sky conditions. Using this framework of experimental comparison will lead to improvements of illumination models as the computer graphics community continues to move towards physically-based measurement and simulations (e.g. in measuring sounds, material properties, and mechanics).

Acknowledgements

This work was supported by Autodesk for energy and daylighting simulation research. Mitsuba was used for all renderings. The authors are grateful to Bruce Walter, Kavita Bala, Steve Marshner, William Philpot, and Adam Arbree who always were willing to provide feedback and guidance. We especially wish to thank Kevin Pratt, Lars Schumann, and Hurf Sheldon who assisted building the device.

References

- ABBOT, C., ALDRICH, L., AND FUND, S. I. H. 1916. *The pyranometer—an instrument for measuring sky radiation*. No. v. 66, nos. 1-18 in Smithsonian miscellaneous collections. Smithsonian institution.
- ACHARYA, P., ANDERSON, G., BERK, A., BERNSTEIN, L., CHETWYND, J., HOKE, M., AND LEWIS, P., 2003. Band model method for modeling atmospheric propagation at arbitrarily fine spectral resolution, May 22. US Patent App. 09/838,801.
- BRUNETON, E., AND NEYRET, F. 2008. Precomputed atmospheric scattering. *Comput. Graph. Forum* 27, 4 (June), 1079–1086. Special Issue: Proceedings of the 19th Eurographics Symposium on Rendering 2008.
- CIE. 1994. *Guide to Recommended Practice of Daylight Measurement*. CIE technical report. CIE.
- DARULA, S., KITTLER, R., AND ROAD, D. 2002. Cie general sky standard defining luminance distributions. *Moon*, 11–13.
- DE BARY, E., AND ESCHELBACH, G. 1974. The ratio of primary scattering to total scattering of sky radiance. *Tellus* 26, 6, 682–690.
- DEBEVEC, P. 1998. Rendering synthetic objects into real scenes: Bridging traditional and image-based graphics with global illumination and high dynamic range photography. In *Proceedings of the 25th Annual Conference on Computer Graphics and Interactive Techniques*, ACM, New York, NY, USA, SIGGRAPH '98, 189–198.
- DIEZ-MEDIAVILLA, M., DE MIGUEL, A., AND BILBAO, J. 2005. Measurement and comparison of diffuse solar irradiance models on inclined surfaces in valladolid (spain). *Energy Conversion and Management* 46, 1314, 2075 – 2092.
- ELEK, O., AND KMOCH, P. 2010. Real-time spectral scattering in large-scale natural participating media. In *SCCG '10: Proceedings of the 26th Spring Conference on Computer Graphics*, ACM, New York, NY, USA, H. Hauser and R. Klein, Eds., 77–84.
- GRYNBERG, A. 1989. Validation of radiance. Tech. Rep. LBID-1575, July.
- GUEYMARD, C. 1995. SMARTS, A Simple Model of the Atmospheric Radiative Transfer of Sun- shine: Algorithms and Performance Assessment. *Florida Solar Energy Center Technical Reports FSEC-PF-270-95*.
- HABER, J., MAGNOR, M., AND SEIDEL, H.-P. 2005. Physically-based simulation of twilight phenomena. *ACM Trans. Graph.* 24, 4 (Oct.), 1353–1373.
- HESS, M., KOEPKE, P., AND SCHULT, I. 1998. Optical Properties of Aerosols and Clouds: The Software Package OPAC. *Bulletin of The American Meteorological Society* 79, 831–844.
- HOFFMAN, N., AND PREETHAM, A. J. 2003. *Rendering outdoor light scattering in real time*. 337–352.
- HOSEK, L., AND WILKIE, A. 2012. An analytic model for full spectral sky-dome radiance. *ACM Trans. Graph.* 31, 4 (July), 95:1–95:9.
- HOSEK, L., AND WILKIE, A. 2013. Adding a solar-radiance function to the hosek-wilkie skylight model. *IEEE Computer Graphics and Applications* 33, 3, 44–52.

- INANICI, M., AND GALVIN, J. 2004. Evaluation of high dynamic range photography as a luminance mapping technique.
- INEICHEN, P., MOLINEAUX, B., AND PEREZ, R. 1994. Sky luminance data validation: Comparison of seven models with four data banks. *Solar Energy* 52, 4, 337 – 346.
- ISO, AND CIE. 2004. *Spatial Distribution of Daylight - CIE Standard General Sky*. ISO 15469:2004 (E)/CIE S 011/E:2003. ISO/CIE.
- JAKOB, W., 2010. Mitsuba renderer. <http://www.mitsuba-renderer.org>.
- KARAYEL, M., NAVVAB, M., NE'EMAN, E., AND SELKOWITZ, S. 1984. Zenith luminance and sky luminance distributions for daylighting calculations. *Energy and Buildings* 6, 3, 283 – 291.
- KNEIZYS, F. X., SHETTLE, E. P., AND GALLERY, W. O. 1981. Atmospheric transmittance and radiance - The LOWTRAN 5 code. In *Atmospheric transmission*, vol. 277 of *Society of Photo-Optical Instrumentation Engineers (SPIE)*, 116–124.
- LITTLEFAIR, P. J. 1994. A comparison of sky luminance models with measured data from garston, united kingdom. *Solar Energy* 53, 4, 315 – 322.
- LOUTZENHISER, P., MANZ, H., FELSMANN, C., STRACHAN, P., FRANK, T., AND MAXWELL, G. 2007. Empirical validation of models to compute solar irradiance on inclined surfaces for building energy simulation. *Solar Energy* 81, 2, 254 – 267.
- MAYER, B., AND KYLLING, A. 2005. Technical note: The libradtran software package for radiative transfer calculations - description and examples of use. *Atmospheric Chemistry and Physics* 5, 7, 1855–1877.
- MYERS, D. R. 2013. *Solar Radiation: Practical Modeling for Renewable Energy Applications (Energy and the Environment)*. Energy and the Environment. CRC Press.
- NISHITA, T., SIRAI, T., TADAMURA, K., AND NAKAMAE, E. 1993. Display of the earth taking into account atmospheric scattering. In *Proceedings of the 20th Annual Conference on Computer Graphics and Interactive Techniques*, ACM, New York, NY, USA, SIGGRAPH '93, 175–182.
- NISHITA, T., DOBASHI, Y., KANEDA, K., AND YAMASHITA, H. 1996. Display method of the sky color taking into account multiple scattering. In *Proceedings of Pacific Graphics 1996*, Pacific Graphics '96, 117–132.
- NOORIAN, A. M., MORADI, I., AND KAMALI, G. A. 2008. Evaluation of 12 models to estimate hourly diffuse irradiation on inclined surfaces. *Renewable Energy* 33, 6, 1406 – 1412.
- OCHOA, C. E., ARIES, M. B. C., AND HENSEN, J. L. M. 2011. State of the art in lighting simulation for building science: a literature review. *Journal of Building Performance Simulation* 5, 4 (May), 209–233.
- PEREZ, R., SEALS, R., AND MICHALSKY, J. 1993. All-weather model for sky luminance distribution preliminary configuration and validation. *Solar Energy* 50, 3, 235 – 245.
- PREETHAM, A. J., SHIRLEY, P., AND SMITS, B. 1999. A practical analytic model for daylight. In *Proceedings of the 26th annual conference on Computer graphics and interactive techniques*, ACM Press/Addison-Wesley Publishing Co., New York, NY, USA, SIGGRAPH '99, 91–100.
- PUST, N. J., AND SHAW, J. A., 2007. All-sky polarization imaging.
- REINHARD, E., STARK, M., SHIRLEY, P., AND FERWERDA, J. 2002. Photographic tone reproduction for digital images. In *Proceedings of the 29th annual conference on Computer graphics and interactive techniques*, ACM, New York, NY, USA, SIGGRAPH '02, 267–276.
- RICCHIAZZI, P., YANG, S., GAUTIER, C., AND SOWLE, D. 1998. SBDART: A Research and Teaching Software Tool for Plane-Parallel Radiative Transfer in the Earth's Atmosphere. *Bulletin of the American Meteorological Society* 79 (Oct.), 2101–2114.
- SHIRLEY, P., AND CHIU, K. 1997. A low distortion map between disk and square. *J. Graph. Tools* 2, 3 (Dec.), 45–52.
- SLOUP, J. 2002. A survey of the modelling and rendering of the earth's atmosphere. In *Proceedings of the 18th spring conference on Computer graphics*, ACM, New York, NY, USA, SCCG '02, 141–150.
- SOLER, A., AND GOPINATHAN, K. 2000. A study of zenith luminance on madrid cloudless skies. *Solar Energy* 69, 5, 403 – 411.
- STUMPFEL, J., JONES, A., WENGER, A., TCHOU, C., HAWKINS, T., AND DEBEVEC, P. 2004. Direct hdr capture of the sun and sky. In *AFRIGRAPH*, 145–149.
- STUMPFEL, J. 2004. *Hdr lighting capture of the sky and sun*. Master's thesis, California Institute of Technology.
- TOMINAGA, S., AND FUKUDA, T., 2007. Omnidirectional scene illuminant estimation using a multispectral imaging system.
- WARD, G. J. 1994. The radiance lighting simulation and rendering system. In *Proceedings of the 21st annual conference on Computer graphics and interactive techniques*, ACM, New York, NY, USA, SIGGRAPH '94, 459–472.
- WILKIE, A., ULBRICHT, C., TOBLER, R. F., ZOTTI, G., AND PURGATHOFER, W. 2004. An analytical model for skylight polarisation. In *Proceedings of the Fifteenth Eurographics Conference on Rendering Techniques*, Eurographics Association, Aire-la-Ville, Switzerland, Switzerland, EGSR'04, 387–397.
- ZOTTI, G., WILKIE, A., AND PURGATHOFER, W. 2007. A critical review of the preetham skylight model. In *WSCG ' 2007 Short Communications Proceedings I*, University of West Bohemia, V. Skala, Ed., 23–30.